Wearable In-Ear PPG: Detailed Respiratory Variations Enable Classification of COPD

Harry J. Davies, Patrik Bachtiger, Ian Williams, Philip L. Molyneaux, Nicholas S. Peters and Danilo P. Mandic

***Abstract*—An ability to extract detailed spirometry-like breathing waveforms from wearable sensors promises to greatly improve respiratory health monitoring. Photoplethysmography (PPG) has been researched in depth for estimation of respiration rate, given that it varies with respiration through overall intensity, pulse amplitude and pulse interval. We compare and contrast the extraction of these three respiratory modes from both the ear canal and finger and show a marked improvement in the respiratory power for respiration induced intensity variations and pulse amplitude variations when recording from the ear canal. We next employ a data driven multi-scale method, noise assisted multivariate empirical mode decomposition (NA-MEMD), which allows for simultaneous analysis of all three respiratory modes to extract detailed respiratory waveforms from in-ear PPG. For rigour, we considered in-ear PPG recordings from healthy subjects, both older and young, patients with chronic obstructive pulmonary disease (COPD) and idiopathic pulmonary fibrosis (IPF) and healthy subjects with artificially obstructed breathing. Specific in-ear PPG waveform changes are observed for COPD, such as a decreased inspiratory duty cycle and an increased inspiratory magnitude, when compared with expiratory magnitude. These differences are used to classify COPD from healthy and IPF waveforms with a sensitivity of 87% and an overall accuracy of 92%. Our findings indicate the promise of in-ear PPG for COPD screening and unobtrusive respiratory monitoring in ambulatory scenarios and in consumer wearables.**

I. Introduction

MONITORING of respiration is being integrated rapidly into consumer wearables, with respiration rate being a standard feature in many smart watches. Whilst continuous unobtrusive monitoring of respiration rate is a valuable tool in both the consumer and patient health tracking domains, much of the respiratory information that can be derived from breathing waveforms remains untapped. To this end, we explore a relatively new tool for non-invasive respiratory monitoring in the form of in-ear photoplethysmography (PPG). For rigour, we use reference spirometry as a gold standard to test the extraction accuracy of the three major respiratory modes at three different frequencies from in-ear PPG: i) intensity variations, ii) pulse amplitude variations, and iii) pulse interval variations. Furthermore, we compare the spectral respiratory power from simultaneous ear canal PPG and finger PPG recordings across the three major respiratory modes. A novel method for extracting respiratory waveforms from PPG is next presented, which involves a data driven multi-scale algorithm, empirical mode decomposition (EMD) [1]. This waveform extraction technique allows for a simultaneous intrinsic scale-wise analysis of multi-channel data, and is applied to extract resting respiratory waveforms from in-ear PPG in both healthy subjects and patients with breathing disorders, such as chronic obstructive pulmonary disease (COPD) and idiopathic pulmonary fibrosis (IPF). This analysis is shown to allow for the detection of chronic obstructive pulmonary disease from in-ear PPG.

A. Respiration and photoplethysmography

Photoplethysmography (PPG) refers to the non-invasive use of light to detect changes in blood volume by transmitting light through tissue and measuring the amount of light that is absorbed. When more blood is present, more light is absorbed and thus less light is reflected back to the sensor.

When we inspire, a decrease in intrathoracic pressure is created to pull air into the lungs. This decrease in pressure is passed to the central veins and therefore central venous pressure also decreases. This, in turn, increases venous return and drains venous beds at the site of the PPG probe, thus modulating the DC component of the PPG signal [2]. Right ventricular stroke volume also increases with the increased venous flow to the heart, sending more blood to the lungs for the uptake of oxygen. In turn, left ventricular stroke volume is decreased, leading to a decreased pulse amplitude observed through the AC component of PPG [3] [4]. This is accompanied by an increase in heart rate, otherwise known as respiratory sinus arrhythmia (RSA) [5], which causes a decrease in the interval between pulses in the PPG signal. The opposite of these effects can be observed during expiration. Three major respiratory modes are therefore present in PPG during respiration [6]:

1) Respiratory induced intensity variations (RIIVs) which are generated by changes in venous pressure which modulate the DC component of photoplethysmography, and are therefore accessible directly from the raw-PPG signal.
2) Pulse amplitude variations due to changes in left ventricular stroke volume, which can be obtained from the envelope of the AC filtered PPG signal.
3) Pulse interval variations generated through respiratory sinus arrhythmia. These can be obtained by measuring the interval between consecutive pulses.

It should also be noted that there are prominent low frequency variations which also occur in the PPG signal, related to sympathetic tone. These low frequency variations usually peak at 0.1Hz [7] [3], with harmonics at 0.2Hz which can negatively impact the extraction of respiratory signals.

An extensive literature exists on estimating respiration rate from PPG, usually from the finger but also from the forearm [2], wrist [8] and multiple other body positions such as the earlobe, forehead, neck [9] and chest [10]. The PPG yields high respiration rate accuracy in all three PPG respiratory modes [11], in both healthy subjects and subjects with breathing disorders, such as chronic obstructive pulmonary disease

(COPD) and asthma [12]. It should be noted that accuracy decreases at high breathing frequencies, above 0.3Hz [13], which is likely due to a low pass filter effect [14] of the transfer function from thoracic pressure to venous return, and the reality of only having a few pulses per breath to sample from for pulse interval and pulse amplitude variations at higher frequencies.

Moreover, it has been shown that errors across the three respiratory modes are comparable when it comes to calculation of respiration rate [15]. This gives a strong argument for the utility of all three modes given the presence of different artefacts, the variability across subjects and the variability across different respiration frequencies and body positions [16]. Research suggests that the spectral power of respiration in PPG is far larger from regions of the head [17], ear [18] and shoulders [19] than the finger. Furthermore, an analysis on spectral power of the PPG at different body positions, namely the forearm, wrist, finger, forehead and shoulder, indicates that the forearm had the highest respiration power but the lowest pulse power, likely due to its close proximity to large veins which may improve the power of RIIVs induced by venous pressure changes; the shoulder and forehead maintain both high respiratory power and pulse power, while the finger had the lowest respiratory power [19].

With photoplethysmography at the forearm, it has been documented that the respiration induced intensity variations (RIIVs) are effective enough to detect amplitude changes in breathing and also simulated apnea with temporary breath holds [2]. However, changes in duty cycle or higher order statistics such as skewness have not been studied in RIIVs. Moreover, despite errors in respiration rate estimation being similar across the three major PPG respiratory modes, when it comes to the magnitude of respiratory variations, they are far more pronounced in venous return than in changes in stroke volume, usually by an order of magnitude [20]. This, in addition to the fact that the sample frequency of pulse amplitude and frequency variations are limited to the pulse rate, suggests that RIIVs may be superior for detecting detailed waveform changes in respiration.

In terms of sex and age differences in respiratory signals from PPG, literature suggests that the pulse interval variations may be more pronounced in females than in males [16], and more pronounced in the young than in the elderly [21], but that there is no significant difference in the RIIVs with age or sex [22].

B. In-Ear Photoplethysmography

With growing popularity of so called Hearables [23], the ear has come to light as a attractive location for wearable sensors, with its prominence in the ear-EEG [24] [25] and ear-ECG domains [26]. Similarly, the in-ear location is rapidly emerging as a favourable site for wearable photoplethysmography and by extension pulse oximetry, due to many benefits over commonly used finger probes. It has proven accurate at detecting hypoxia [27] and for detecting apnea events during obstructive sleep apnea [28]. Additionally, a significantly faster response time to changes in blood oxygen has been shown from the ear when compared with the finger [29].

In-ear PPG has also been shown to be resistant to changes in blood volume which occur during hypothermia [18], in contrast to commonly used photoplethysmography positions such as the earlobe or the finger. During cold exposure, peripheral areas of the body experience vasoconstriction, whereas the ear canal maintains internal blood flow levels. As previously discussed, current research suggests that PPG from the ear canal is far more sensitive to intensity variations that arise from respiration [18] than the finger PPG, which is inline with similar results for shoulder and forehead PPG [19]. However, this increase in respiratory power has only been documented through respiratory induced intensity variations in the raw PPG signal. To address this issue, we examine the spectral power across all three PPG respiratory modes in both in-ear PPG and finger PPG. Furthermore, in-ear PPG has only been used to estimate respiratory rate [28], but has not been used for insight into the respiratory waveform itself. In this paper we set out to show that in-ear PPG possesses sufficient respiratory waveform information for the screening of obstructive breathing disorders.

C. Change in breathing with COPD

The prevalence of respiratory diseases has grown by 39% in the last 3 decades [30], with nearly 1 in 5 people in the UK having had a diagnosis of asthma, chronic obstructive pulmonary disease or another respiratory illness [31].

Chronic obstructive pulmonary disease (COPD) is a debilitating illness caused by an increased inflammatory response in the lungs which leads to obstructed airflow [32], particularly during expiration. Chronic obstructive pulmonary disease is generally diagnosed with spirometry, by measuring the ratio of volume during forced expiration in one second (FEV_1), against forced vital capacity (FVC), whereby COPD is defined as $FEV_1/FVC<0.7$. This obstruction during expiration leads to an increased respiratory rate (tachypnea), with a decreased inspiration time (T_I) in comparison with the overall breathing time (T_{TOT}). The ratio of T_I/T_{TOT} in COPD, otherwise known as the inspiratory duty cycle, is therefore decreased at rest and during exercise [33] [34], with values of around 0.35 seen at rest compared with 0.42 in healthy patients [33]. This change in duty cycle is a major difference seen in obstructive lung disease when compared to restrictive lung diseases such as idiopathic pulmonary fibrosis (IPF), where, due to the restriction to both inspiration and expiration, the FEV_1/FVC remains higher [35]. Pulmonary fibrosis usually has an increased respiratory rate, and lower respiratory volume, but no significant change to the duty cycle.

Other methods of classifying respiration in COPD include examining the sample entropy of flow signals [36], where the sample entropy decreased with an increasing severity of COPD due to fewer degrees of freedom with constrained breathing. Moreover, in the PPG domain, a combination of pulse, respiration rate, and SpO_2 (derived from pulse oximetry) has been used to predict exacerbations in COPD patients with moderate accuracy [37], and PPG has recently been used to estimate lung compliance in lung disease [38]. To our knowledge, there has not yet been a successful classification

of COPD from PPG-derived respiratory waveforms, and to address this void we both explore the valuable respiratory properties of in-ear PPG and employ these in patients to examine and classify COPD.

II. Materials and Experimental Design

A. Hardware

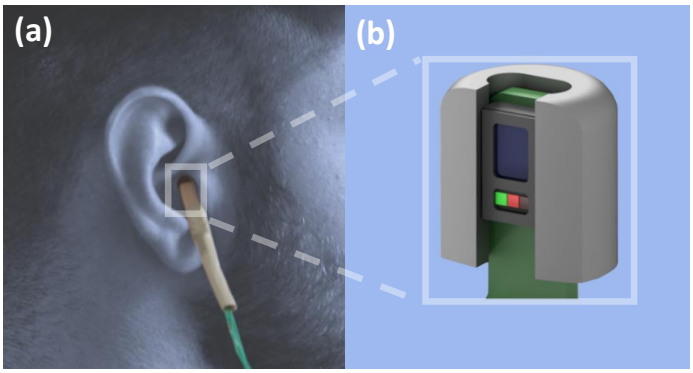

Fig. 1. The in-ear photoplethysmography sensor used in our study. (a) Sensor placement within the ear canal. (b) Zoom-in of the pulse oximetry sensor, with a form factor of a viscoelastic memory foam earbud.

The photoplethysmography sensor used was the MAX30101 digital PPG chip by Maxim Integrated (San Jose, CA, USA), which consists of green (537nm), red (660nm) and infrared (880nm) light emitting diodes as well as a photo-diode to measure the reflected light. In this study, we utilised the infrared light emitting diode for PPG measurements as it gave the strongest signal to noise ratio. The PPG chip was positioned on a thin rectangular printed circuit board with decoupling capacitors and level shifting circuitry that enable digital communication between the 1.8 V and 3 V domains. The chip and corresponding circuitry were neatly covered in heat shrink and embedded in a cut-out rectangular section of a viscoelastic foam earbud [39]. For user comfort, the earbuds were of small, medium and large sizes. The PPG chip, earbud and its placement in the ear are shown in Fig. 1. In the simultaneous in-ear PPG and finger PPG recordings, the same sensor was secured to the right index finger. The PPG sensors were wired to a purpose built circuit board which stored the data on an SD card.

For simultaneous spirometry and in-ear PPG recordings, a SFM3200 flow meter by Sensiron (Stäfa, Switzerland) was used to measure breathing flow with an airtight connection to a tube into which the participant breathed, whilst a nose clip restricted nasal breathing. The SFM3200 was connected to an Arduino Uno by Arduino (Somerville, MA, USA) which recorded the flow rate values. The Arduino was also used to send out electrical pulses to the PPG recording circuit at semi-regular time intervals, so that the two data streams of PPG and airflow could be time aligned.

B. Experimental Design

1) Simultaneous spirometry and in-ear PPG: Simultaneous in-ear PPG and spirometry was used to evaluate presence of respiratory frequencies in the three respiratory modes of intensity, pulse amplitude and pulse interval. This was achieved across three different frequencies corresponding to slow, moderate and fast breathing rates. Furthermore, simultaneous in-ear PPG and spirometry recordings were used to evaluate the extraction of the examined breathing waveforms: i) normal breathing and ii) breathing with a duty cycle typical to severe chronic obstructive pulmonary disease (COPD). In both the cases of frequency and flow waveform, the spirometer served as the ground truth. The participant in these recordings was a healthy male aged 25 years. The participant had the in-ear photoplethysmography sensor placed in the right ear canal, whilst breathing into the spirometer. In both cases of breathing at different frequencies and with different characteristic waveforms, the subject was informed of when to inspire and expire using a timed on-screen animation. For the frequency recordings, the animation aided the subject in breathing at frequencies of 0.18Hz, 0.25Hz and 0.33Hz, corresponding to 10.8 breaths per minute, 15 breaths per minute and 20 breaths per minute, respectively. The subject adhered to each frequency for 2 minutes, with 30 seconds rest between different frequencies. For the simulated low inspiratory duty cycle breathing, the base frequency was 0.2Hz and the subject adhered to a breathing timing ratio that was 1:3 inspiration to expiration, for 120 seconds.

2) Simultaneous in-ear and finger PPG: The participants in the recordings were 14 healthy subjects (7 males, 7 females) aged 19 - 38 years. Two PPG sensors were used per subject, the first safely secured within the right ear canal, as shown in Fig. 1, and the second secured to the right index finger. Subjects were in a seated position and were instructed to breathe normally for 120 seconds, whilst photoplethysmography was recorded from simultaneously from both the ear and finger. Out of the 14 subjects, 3 subjects were discarded from analysis as they showed no clear respiratory peak in the frequency domain. The 11 subjects used for analysis consisted of 6 males and 5 females aged 19 - 28 years.

3) Resting recordings in older healthy subjects and patients with breathing disorders: The participants in these recordings were split up into 2 groups, an older healthy subset of 4 subjects (2 males, 2 females) aged 56 - 62 years, and a subset of 6 subjects with respiratory disease (3 males, 3 females) aged 53 - 88 years. Out of the patients with respiratory disease, 4 patients had chronic obstructive pulmonary disease and 2 patients had idiopathic pulmonary fibrosis. Continuous PPG was measured from the ear canal of subjects at rest for 2 minutes using our in-ear PPG sensor.

4) Artificially obstructed breathing: The participants in these recordings were 6 healthy subjects (4 males, 2 females) aged 23 - 30 years. Participants were asked to breathe in through a tube of internal diameter 8mm and length 300mm, and breathe out through a tube of internal diameter 5mm and length 300mm, giving a ratio of resistance from inspiration to expiration of $\frac{25}{64} \approx 0.4$. The tubes were linked with one-way valves in opposite directions so that breathing would automatically switch between the two tubes when switching from inspiration to expiration [40]. Continuous PPG was measured from the ear canal of subjects whilst they breathed

through the tubes for 2 minutes.

The recordings were performed under the IC ethics committee approval JRCO 20IC6414, and the NHS Health Research Authority 20/SC/0315. All subjects gave full informed consent.

III. Signal Processing

A. Extraction of Respiratory Modulations from PPG

The three major respiratory modes in photoplethysmography are: i) respiration induced intensity variations (RIIVs) which are accessible from the raw PPG, ii) pulse amplitude variations and iii) pulse interval variations, both accessible from the AC component of PPG. The extraction of the RIIV waveforms can be achieved via band-pass filtering or by adaptive methods such as empirical mode decomposition which will be described in full in the next section. However, for the purpose of spectral comparisons, the RIIV can be observed by taking the periodogram of the unfiltered PPG signal, whereby the signal is first detrended to remove the drifts and ensure that the periodogram is not biased at 0Hz.

To extract the AC component of the PPG signal, the detrended PPG was band-pass filtered between 0.9 and 30Hz. Peaks and troughs were then extracted from the pulse signal using the MATLAB by MathWorks (Natick, MA, USA) function *findpeaks*, with a minimum peak prominence of 150 arbitrary units. For the pulse amplitude variations, the envelope of the pulse signal was calculated by interpolating the peaks at 62.5Hz, and interpolating the troughs at 62.5Hz, and then summing up their absolute value. The time values of the troughs were used for the pulse interval variations as, due to the characteristic pulse waveform from the ear [29], the troughs are less sensitive to noise. The pulse interval signal was calculated as the time between consecutive pulses at the time point of each trough, and interpolated at 62.5Hz to match the sampling frequency of the PPG signal. Fig. 2 shows exemplar periodograms of the three respiratory modes, indicating that the normalised power spectral density has good adherence to the ground truth spirometry across all respiratory modes and across the three respiratory frequencies of 0.18Hz, 0.25Hz and 0.33Hz. The largest disparity between the estimated frequency and ground truth was an error of 0.003Hz (0.18 breaths per minute) that occured with the pulse interval mode at 0.33Hz breathing. The periodograms were, however, taken over long time periods of 100 seconds and the recordings were performed with minimal movement, providing an ideal situation for good frequency adherence. Over shorter time periods and with motion artefacts, adherence to the ground truth periodogram would be lower.

B. Respiratory Power Comparisons: Ear vs Finger

From the 120 second photoplethysmography recordings of normal breathing, the two modes of *pulse amplitude variations* and pulse interval variations were extracted from the ear and finger as described in the previous subsection. The analysis considered the final 84 seconds (5250 samples) in an attempt to mitigate the conscious effects on breathing that can occur when first being told to breathe normally. All three modes were detrended to remove the mean, and power spectra of the three modes were then assessed for a shared respiratory peak. The recording was discarded if there was no clear shared peak present across modes on both the ear and finger recordings. A clear respiratory peak was observed in 11 out of the 14 recorded subjects. The normalised peak value was calculated by taking the power spectral density (PSD) value of the respiratory peak and dividing it by the sum of the power spectral density from 0Hz to 2Hz. The respiratory PSD ratio was then calculated by dividing the normalised peak from the ear by the normalised peak from the finger, and $\log_{10}$ of the ratio was taken to make the distribution of ratios proportional in each direction. Accordingly, a negative value represented a greater relative respiratory power from the finger, a positive value represented a greater relative respiratory power from the

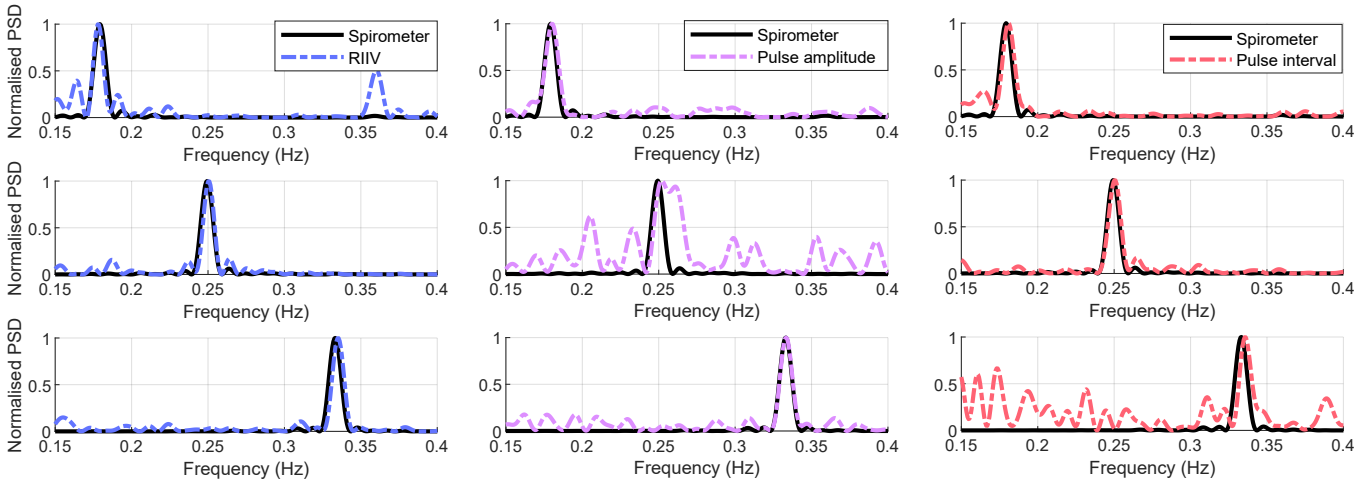

Fig. 2. Normalised power spectral density (PSD) between 0.15 and 0.4Hz of each respiratory mode from in-ear PPG: Respiration induced intensity variations (blue, left), pulse amplitude variations (purple, middle) and pulse interval variations (red, right). The normalised PSD for each recording and respiratory mode is compared with the normalised PSD of the ground truth spirometry in each plot, which provides the true frequency distribution of respiration for that recording. The top row corresponds to recordings with a breathing rate of 0.18Hz, with the middle row and bottom row to 0.25Hz and 0.33Hz respectively.

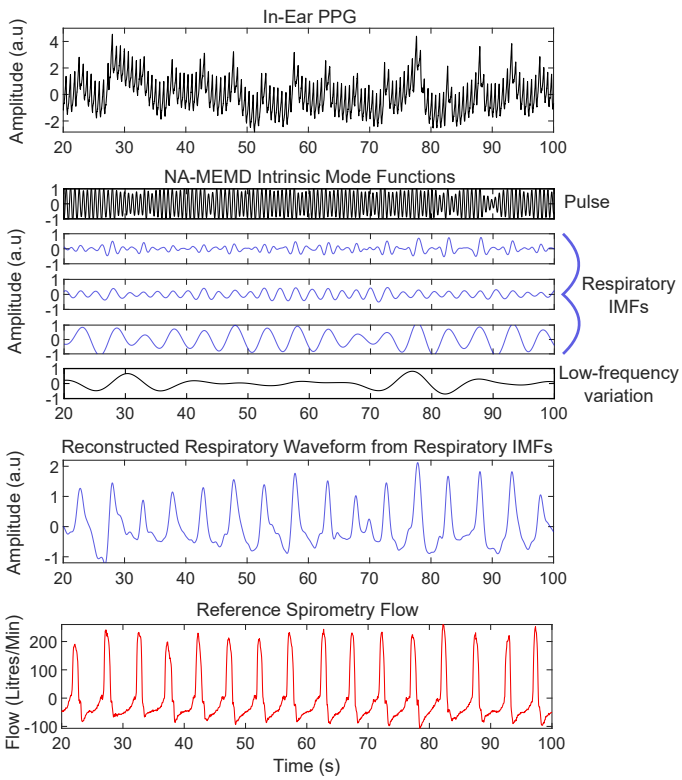

Fig. 3. Noise assisted multivariate empirical mode decomposition (NA-MEMD) of in-ear PPG for a subject breathing with an atypical 1:3 inspiration to expiration time ratio. Indicated are the detrended in-ear PPG (top, black), the breakdown of the in-ear PPG into intrinsic mode functions (top middle) with the respiratory IMFs highlighted in blue, the reconstructed in-ear PPG respiratory waveform (bottom middle, blue) and the reference spirometry flow signal (bottom, red). For convenience, the PPG waveform is flipped so that peaks correspond to inspiration and troughs correspond to expiration.

ear, and a value of zero represented no difference between the two recording sites. This method is similar to methods previously employed in the literature, with the difference in that it focuses on a defined respiratory peak rather than on overall power in the frequency band. This choice was made as in general especially with the respiration induced intensity variations, much of the power in the respiration frequency band can be from higher harmonics of low frequency variations. Moreover, normalising by the sum of the power spectral density helped to mitigate differences in signal quality that could occur from inadequate placement of either sensor. Importantly, our analysis looked at all three respiratory modes, rather than just the respiration induced intensity variations.

C. Empirical Mode Decomposition for Respiration

Empirical mode decomposition (EMD) employs a nonlinear data driven filter-bank structure to deconstruct time domain signals into data-adaptive narrow-band amplitude and frequency (time series) components, known as intrinsic mode functions (IMFs) [1]. Since the IMFs obtained by empirical mode decomposition are data driven and thus physically meaningful, empirical mode decomposition has proven effective at decomposing nonstationary and multi-scale physiological data, such as electroencephalography (EEG) into different frequency bands [41] [42] and at extracting respiration rate from PPG [43].

Within the single channel EMD algorithm [1], firstly a proto-IMF is defined, and all local maxima and minima of the signal are extracted and interpolated separately to give a signal envelope. The mean between these envelopes is calculated, and removed from the proto-IMF. These steps of envelope removal are repeated until the proto-IMF satisfies the following conditions: i) the number of extrema and zero crossings must differ by at most one (giving an oscillatory signal) and ii) at any point the mean value of the maxima and minima envelope must be zero. When the proto-IMF satisfies these conditions it represents a valid IMF. The steps are repeated again and more IMFs are extracted until a monotonic residue or trend is left, or until a set number of IMFs has been reached.

Multivariate EMD (MEMD) [44] generalises the standard EMD algorithm to multiple channels and is commonly used in scenarios such as EEG where multiple channels convey variants of the same EEG information. A hypersphere of uniformly sampled points is generated based on a low-discrepancy Hammersley sequence and these Q points are used to perform single-dimensional projects of the signal along the Q direction vectors. The envelopes of those single-dimensional projections are extracted and the mean of these envelopes across the Q direction vectors is taken [1]. As with the original EMD algorithm, these mean envelopes are successively removed from the input signal and IMFs are extracted for each variate when the IMF conditions are satisfied. The conditions for IMFs are modified slightly in MEMD by not imposing the condition for the number of extrema and zero crossings varying by at most one [45], as extrema cannot be properly defined for multivariate signals.

Further, it has been shown that the frequency localisation of MEMD can be improved by adding adjacent independent noise channels to MEMD, a concept called noise assisted multivariate empirical mode decomposition (NA-MEMD) [44]. The NA-MEMD performs especially well on real world physiological data, helping to extract physically meaningful intrinsic mode functions.

To extract respiratory waveforms from PPG, we employed the raw photophlethysmography signal, the pulse interval variations and the pulse amplitude variations as the three main channels in NA-MEMD, given that the commonality between the intensity mode, the pulse amplitude mode and the pulse interval mode is the respiratory information. Therefore, rather than using different recording channels as our inputs, our main inputs are instead all derived from the same PPG signal. Five white Gaussian noise channels are added to improve frequency localisation and reduce the mode mixing between the IMFs. This produces IMFs for each of the three respiratory modes. Only the IMFs for the raw PPG signal were used to reconstruct the respiratory waveform, given that the intensity based modulations are not limited in sample rate to the pulse frequency and therefore contain more detailed high frequency respiratory information. A respiratory IMF was defined as an IMF with over a third of its spectral power between 0.2Hz and 0.6Hz, allowing higher frequency respiratory detail to

TABLE I
SUMMARY OF FEATURES USED FOR CLASSIFICATION OF COPD

Category	Features
COPD based	skewness, duty cycle, $max - \lvert min \rvert$, normalised $max - \lvert min \rvert$ [†]
General	Standard deviation, kurtosis, spectral skewness, breathing frequency

[†] Normalisation corresponds to division by the standard deviation.

be captured. The respiratory IMFs were then summed to reconstruct the respiration signal. This achieved physically meaningful respiratory waveforms which vary both in amplitude and frequency across the respiratory band.

An example of NA-MEMD decomposition and reconstruction is shown in Fig. 3. The subject adhered to a 1:3 inspiration to expiration time ratio, similar to respiratory waveforms typical of severe chronic obstructive pulmonary disease. It can be seen that despite the lowest frequency respiratory IMF capturing the base frequency of respiration, it lacks the detail captured in the higher frequency IMFs which help to illuminate the difference in inspiration to expiration time ratio. This is an argument for using methods such as empirical mode decomposition over standard filter banks when trying to extract physically meaningful respiratory waveforms.

D. Classification of COPD

For the classification of chronic obstructive disease we focused extracting features based on the COPD waveform, given that we desire to be able to classify COPD not just in comparisons with healthy data but relative to other respiratory diseases. Whilst respiration frequency itself is an important feature in assessing respiratory health, both COPD and pulmonary fibrosis lead to an increase in breaths per minute, making it a poor feature for distinguishing between the two when used alone.

Six in-ear PPG recordings were used from ear finger comparisons and labelled as young and healthy. Therefore in total there were 6 young healthy subjects aged 21 - 28 years, 4 older healthy subjects aged 56-62 years, 4 subjects with COPD aged 55 - 88 years and 2 subjects with idiopathic pulmonary fibrosis (IPF) aged 61 and 68 years. The 120 second recordings of PPG data from each subject were trimmed to remove motion artifacts occurring at the start and end of the recordings, and pulse interval and pulse amplitude variation signals were extracted. The NA-MEMD was then performed on the PPG, pulse interval and pulse amplitude signals for each subject independently. Respiratory signals were then reconstructed from the respiratory intrinsic mode functions, and 15-second epochs without the presence of motion artifacts were selected. Each 15-second epoch was rounded off so that the number of breathing cycles was an integer; in this way, 15 segments were extracted for COPD, 10 for IPF, 18 for young healthy and 16 for older healthy, resulting in a total of 59 segments. During inspiration, the raw PPG decreases in intensity, and therefore for convenience the waveforms were flipped so that peaks represented peak inspiration, and troughs represented peak expiration.

Features were chosen by accounting for the principle that COPD mainly obstructs expiration, and thus expiration takes up a larger proportion of the total breathing time, while resting inspiratory flow rates are usually higher than expiratory flow rates. The skewness, duty cycle and the difference between the maximum value and the absolute of the minimum value were extracted as COPD related features. Skewness is defined as

$$S(\mathbf{y}) = \frac{E(\mathbf{y}-\mu)^3}{\sigma^3} \tag{1}$$

where $S(\mathbf{y})$ denotes the skewness of a signal $\mathbf{y}$, $E(x)$ represents the expected value of x, μ is the mean of the signal $\mathbf{y}$, and σ is the standard deviation of $\mathbf{y}$. Distributions with a longer positive tail than negative tail therefore have a positive skewness, and distributions with a longer negative tail have a negative

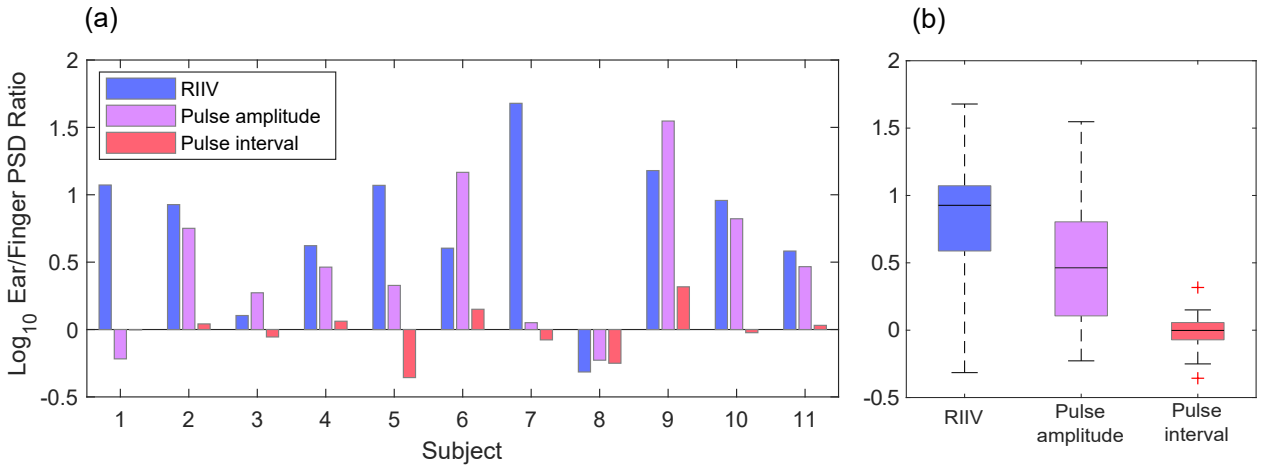

Fig. 4. The $\log_{10}$ of the respiratory power spectral density ratio between the ear and finger, for each respiratory mode of respiration induced intensity variations (RIIV) (blue), pulse amplitude variations (purple) and pulse interval variations (red). (a) The $\log_{10}$ ratios for each respiratory mode presented for all 11 subjects. (b) Boxplots showing the distribution of $\log_{10}$ ratios for each respiratory mode. Values of zero represent equal relative respiratory power for both the ear and finger, whereas values of 1 represent a 10-fold increase in relative respiratory power from the ear and values of -1 represent a 10-fold decrease in relative respiratory power from the ear.

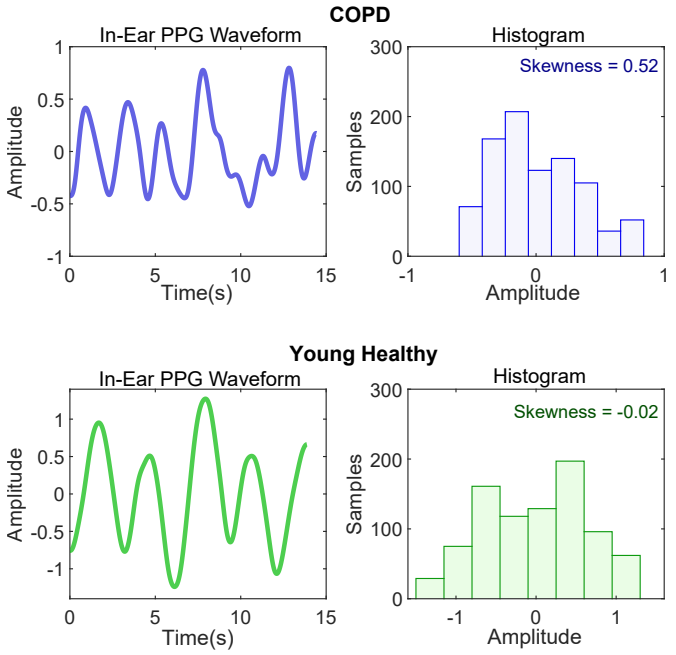

Fig. 5. Exemplar in-ear PPG respiratory waveforms and their corresponding probability density estimates shown in the form of histograms, for the case of a patient with COPD (top, blue) and a young healthy subject (bottom, green). Skewness values for each presented waveform are shown in the histogram plots, with a skewness of 0.52 for the COPD in-ear PPG waveform and -0.02 for the young healthy in-ear PPG waveform.

skewness. Similarly, distributions that are symmetrical have zero skewness.

For our implementation, duty cycle was defined as time spent in inspiration divided by time spent in expiration. Given that the respiration induced intensity variation of PPG is a proxy for flow rate and assuming the mean flow rate is zero, time spent above the mean of the flipped waveform corresponds to inspiration, and time spent below the mean to expiration. Thus, inspiratory duty cycle was calculated by dividing the number of samples above the mean by the number of samples below the mean as follows

$$D(\mathbf{y}) = \frac{\sum_{n=1}^{N} H(y(n)-\mu)}{\sum_{n=1}^{N} H(\mu - y(n))} \tag{2}$$

where $D(\mathbf{y})$ corresponds to the duty cycle of a signal $\mathbf{y}$, N represents the sample number, μ is the mean of the signal $\mathbf{y}$, and H represents the Heaviside function. Overall, a total of 8 features were used for classification, and are summarised in Table I.

For classification, features were used to train a random forest classifier, employed using the scikit-learn Python toolbox [46]. For the random forest base, the number of trees was set to 50, the class weight was set to 'balanced subsample' and the maximum number of features was set to 3. Binary classification was performed with the COPD data being labeled as such, and the young healthy, older healthy and IPF data being labelled as non-COPD. Both leave-one-segment-out and leave-one-subject-out cross validation methods were used. In the case of leave-one-segment-out, a summed confusion

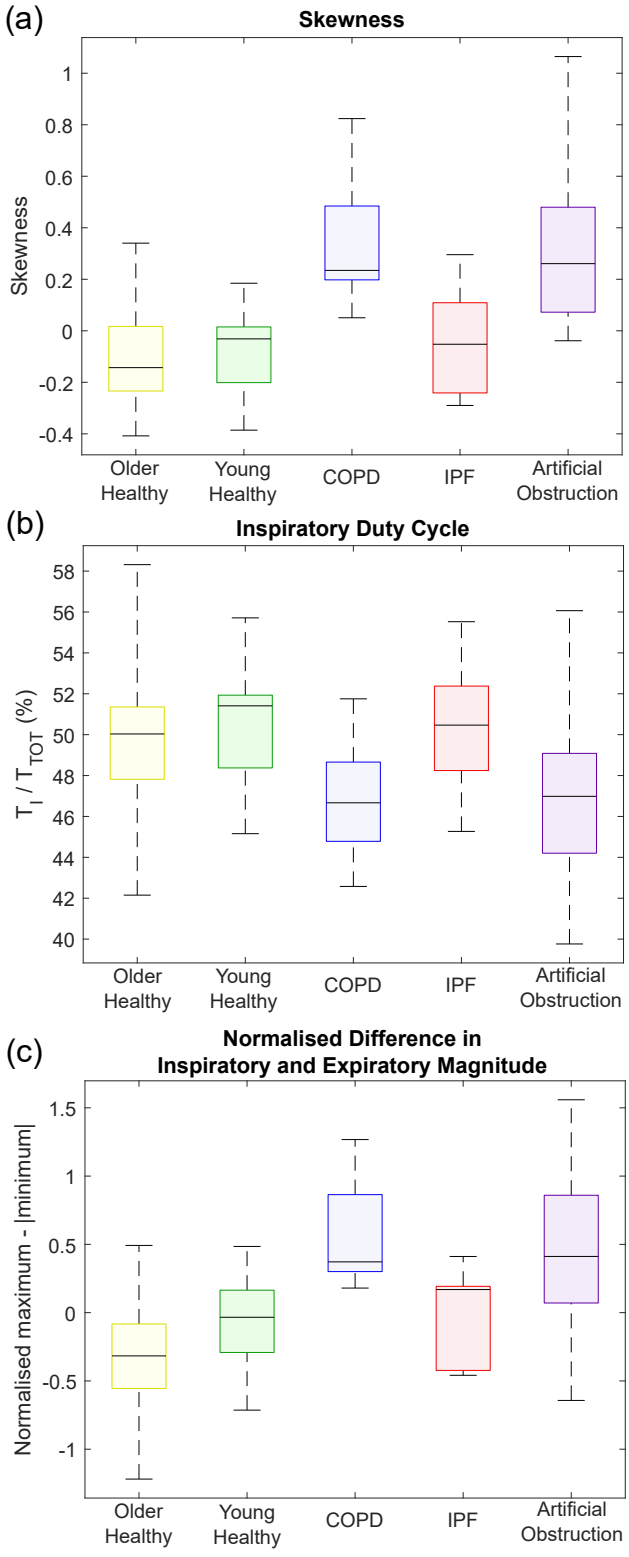

Fig. 6. Boxplots of COPD related features extracted from in-ear PPG recordings for older healthy subjects (yellow, 16 segments), young healthy subjects (green, 18 segments), patients with COPD (blue, 15 segments), patients with IPF (red, 10 segments) and healthy subjects with artificially obstructed breathing (purple, 23 segments). (a) Boxplots of skewness defined in (1). (b) Boxplots of inspiratory duty cycle defined in (2). (c) Boxplots of the normalised difference in inspiratory and expiratory magnitude, defined in Table I as the normalised maximum from which the absolute value of the minimum is subtracted.

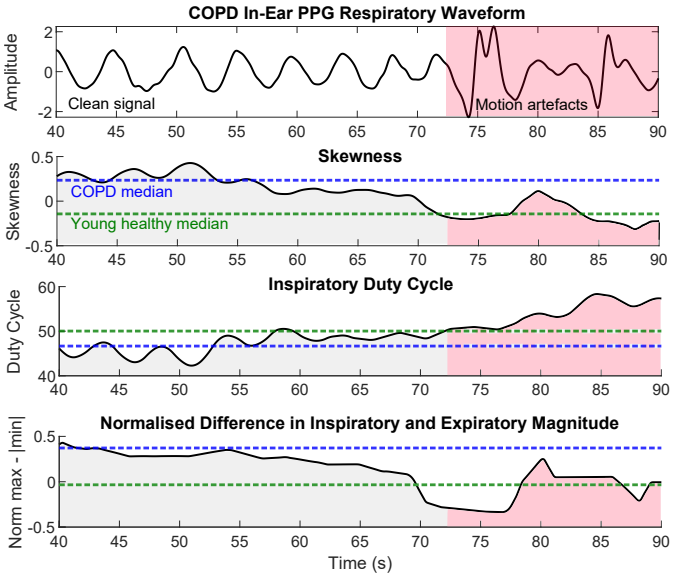

Fig. 7. An exemplar in-ear PPG derived COPD respiratory waveform, with the corresponding COPD features calculated with a sliding 500 sample (8 second) window. For each feature, highlighted with dotted lines are medians from the COPD recordings (blue) and the medians from the young healthy data set (green). The pink shaded section highlights the presence of motion artefacts in the data, and the corresponding distortion to the calculated features.

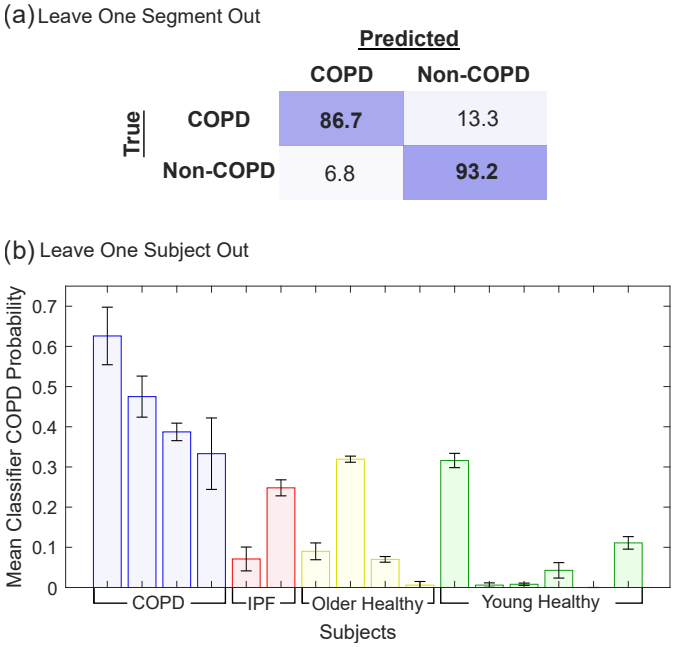

Fig. 8. Classification of COPD from in-ear PPG respiratory waveforms. (a) The mean confusion matrix for leave-one-segment-out cross validation, with the rows corresponding to the true COPD and non-COPD allocations, and the columns corresponding to the predictions of COPD and non-COPD. (b) The mean COPD probabilities extracted from the random forest classifier across each segment for a given subject, and ensemble averaged over 5 realisations. The error bars correspond to the standard deviation of the segment mean over 5 realisations. The COPD subjects are designated in blue, IPF in red, older healthy in yellow and young healthy in green.

matrix was used to evaluate performance, and in the case of leave-one-subject-out the mean classifier probability for COPD was taken over all segments for that subject, and an ensemble average was taken over 5 different train-test realisations.

IV. Results

A. Spectral Power of In-Ear PPG vs Finger PPG

The $\log_{10}$ ear to finger respiratory power ratios for the three respiratory modes of respiration induced intensity variations (RIIVs), pulse amplitude variations and pulse interval variations for 11 subjects are presented in Fig. 4(a). The boxplots presented in Fig. 4(b) show median $\log_{10}$ ratio values of 0.927 for RIIV, 0.463 for pulse amplitude variations and -0.002 for pulse interval variations, corresponding to an average of an 8.5-fold increased RIIV power from the ear compared to the finger, a 2.9-fold increase in pulse amplitude power from the ear and no change in the power of the pulse interval variation between the ear and the finger. A one sample t-test rejected the null-hypothesis that the $\log_{10}$ ratios had a distribution mean of zero in the case of the RIIV and pulse amplitude ratios ($p = 0.0008, p = 0.01$) and did not reject the null hypothesis in the case of the pulse interval power ratios ($p = 0.79$). When comparing the ratios and normalised respiratory peak values across the sexes (5 female, and 6 male) the only significant difference found was an increased pulse interval variation power in the finger in females compared with males ($p = 0.04$) and whilst an increased pulse interval variation power was also seen in the ear in females, it was not significant ($p = 0.15$).

B. Classification of COPD from In-ear PPG

The COPD data in general showed higher skewness than non-COPD data. Fig. 5 exemplifies that the COPD waveform is more likely to have higher amplitude inspiratory peaks when compared with expiratory troughs, thus giving the waveform distribution a positive tail and therefore a positive skew as highlighted through the histograms. The distribution of skewness between older healthy, young healthy, COPD and IPF is summarised in the boxplots in Fig. 6(a), and shows that overall the skewness of COPD segments tends to be higher with a median of 0.23 and an interquartile range of 0.20 to 0.48, compared with an older healthy median of -0.14 and IQR of -0.23 to 0.02, a young healthy median of -0.03 and IQR of -0.20 to 0.02 and an IPF median of -0.05 and IQR of -0.24 to 0.11. The change in duty cycle in COPD from in-ear PPG was less pronounced than the difference in skewness, but in general T_I/T_{TOT} was lower in COPD as shown in Fig. 6(b). The median duty cycle in COPD was 46.7%, compared with 50.0%, 51.4% and 50.5% in the older healthy, young healthy and IPF subjects, respectively. The distribution of normalised difference in inspiratory and expiratory magnitude was similar to skewness, with values above zero corresponding to increased inspiratory magnitude and values below zero corresponding to increased expiratory magnitude. Fig. 6(c) shows that COPD skewness values trend higher with a median of 0.37 and an IQR of 0.30 to 0.86, compared with an older healthy median of -0.32 and IQR of -0.56 to -0.08, a young healthy median of -0.03 and IQR of -0.29 to 0.16 and an IPF median of 0.17 and IQR of -0.42 to 0.19. Artificial obstruction mirrored COPD across all

features, with a median skewness of 0.26, a median duty cycle of 47.0% and a median normalised difference in inspiratory and expiratory magnitude of 0.41, compared to median values of 0.23, 46.7% and 0.37 in COPD.

All features were calculated on clean segments of data, with segments with motion artefacts being ignored. Fig. 7 highlights that motion artefacts can distort the features, with an example of feature calculation in an artefact corrupted COPD recording. It is shown that features diverge from what is expected for COPD towards what is expected for young healthy participants when a motion artifact is present, which in this case would lead to miss-classification.

Average classification accuracy for leave-one-segment-out cross validation was 92%, with class specific accuracy of 87% for COPD, and 93% for non-COPD. These results are presented in the confusion matrix in Fig. 8(a). Moreover, classification of COPD had a precision of 81% and an F-score of 84%. In the leave-one-subject-out cross validation results, the COPD probability was extracted from the random forest classifier and the mean was calculated across testing segments for each subject, with the ensemble average of this probability then taken over 5 realisations. The 4 COPD subjects had the 4 highest classifier probabilities of COPD, as shown in Fig. 8(b). In both cases of leave one subject and leave-one-segment-out, the 2 most important features for classification, based on the reduction of tree impurity in the random forest, were the skewness and the normalised difference between the maximum and absolute minimum.

V. Discussion

A. Spectral Power of In-Ear PPG vs Finger PPG

The increased respiration induced intensity variation power of roughly 8.5-fold that we see from the ear over the finger is in good agreement with Budidha *et al* [18], Nilsson *et al* [19] and Shelley *et al* [17], but is in contrast to the findings of Charlton *et al* [21]. In addition, we also see in increased spectral power of pulse amplitude variations due to respiration from the ear, again in contrast to Chartlon *et al* [21], and no change in power for pulse interval variations. In the case of the work by Charlton *et al*, the authors explain that the difference may be due an increased signal to noise ratio from the finger sensor, whereas we have accounted for differences in signal quality in our calculations. One possible explanation for the increased power that we see in the amplitude variations from the ear is that the ear canal vasculature is in close proximity to the carotid artery, and therefore a more exaggerated pulse amplitude variation might be expected.

Moreover, we do not see a significant difference in RIIVs between the sexes for the ear or finger sensors which is in agreement with Nilsson *et al* [22]. Similarly we do not see a significant difference in the pulse amplitude variations between sexes from the ear and finger, and we do not see a significant difference in the pulse interval variations between sexes from the ear. We do, however, see a significantly higher respiratory power for pulse interval variations in the finger from females, which is in agreement with Li *et al* [16].

B. Classification of COPD from In-ear PPG

In the extracted in-ear PPG respiratory waveforms, we found an increased skewness of the data distribution towards inspiration, higher inspiratory magnitudes compared with expiratory magnitudes and decreased inspiratory duty cycle in those with COPD, compared with young healthy subjects, older healthy subjects and patients with IPF. Theoretically, these differences were expected, given COPD manifests itself in obstruction to expiration which results in a lower FEV_1/FVC when testing with spirometry, and therefore in a shorter time spent inspiring and a higher peak inspiratory flow compared with expiratory flow at rest. Importantly, when breathing was artificially obstructed with tubes that restricted expiration more than inspiration, the analysis showed the same trends as with COPD. This provides further justification that the chosen features discriminate obstructive breathing disorders. The duty cycle differences were not as pronounced from the ear-PPG as those from chest wall measurements in the literature [33] [34], and were higher for all COPD and non-COPD subjects. In the case of the recorded 1:3 inspiration to expiration example, presented in Fig. 3, the flow data had a inspiratory duty cycle 26%, whereas the in-ear PPG extracted waveform had a calculated duty cycle of 37%. Similarly, flow data had a skewness = 1.5 compared with a skewness = 0.9 in the in-ear PPG waveform. This is evidence for waveform differences in breathing being less pronounced from the in-ear PPG than in the ground truth air flow, and is a possible explanation for why the differences from the ear waveforms recorded in COPD patients are less pronounced than the chest wall measurements in the literature. A similar duty cycle and skewness to the extracted in-ear PPG waveforms was achieved by low-pass filtering the spirometry flow data in Fig .3, with a cut off frequency of 0.33Hz. This is evidence that the reduction in COPD differences shown from in-ear PPG is likely caused by the transfer function from thoracic pressure to venous return which has low-pass filter effects [14]. This effect may also be exaggerated by patients with COPD on average having higher resting respiration frequencies.

Analysis of data corrupted by artefacts, shown in Fig. 7, highlights that motion artefacts can indeed distort the extracted features, and thus for the classification of COPD it is recommended that artefact corrupted segments are discarded. This however, does not affect the utility of the proposed methodology, as with this method classification can be performed on data recorded at rest where artefacts are far less common than during movement such as walking. Furthermore, with only a few clean breathing cycles required to achieve an accurate prediction, the negative impact of artefacts is further reduced. Motion artefacts are generally of a broadband nature, with a peak frequency that is at least an order of magnitude higher than the peak frequency of PPG derived respiratory waveforms; this makes it straightforward to identify and reject artefact-corrupted segments.

Using features extracted from in-ear PPG waveforms segments that were less than 15 seconds long, a random forest classifier was able to distinguish between COPD and non-COPD with a specificity of 87% and overall accuracy of

92% in leave-one-segment-out cross validation. Moreover, the fact that the highest mean classifier probabilities all occurred in COPD subjects with leave-one-subject-out cross validation demonstrates that the in-ear PPG features, described in this paper, are robust enough to generalise across COPD patients even with only 3 training subjects. Notably, COPD was classified against the young healthy data, older healthy data and IPF patient data, which reinforces our claim that we are detecting COPD and not just differences that could occur in general breathing disorders or with age. Importantly, this indicates that the respiratory variations detected in the in-ear PPG are strong enough to preserve information that goes beyond the respiration frequency. With more subjects, the accuracy and ability of the model to generalise would likely increase further.

VI. Conclusion

We have demonstrated the principle and robustness of in-ear PPG as a tool for detecting respiration frequency. It has been shown to exhibit increased spectral power over the finger PPG due to respiration for both respiration induced intensity variations and pulse amplitude variations. Further, we have introduced a novel method for extracting respiratory waveforms from PPG, based on noise assisted multivariate empirical mode composition (NA-MEMD), and have proven that so extracted in-ear PPG breathing waveforms contain sufficient information to detect differences that occur with obstructive breathing disorders such as chronic obstructive pulmonary disease (COPD). This has been further validated quantitatively when classifying COPD against healthy subjects and subjects with pulmonary fibrosis, and through comparison with artificially obstructed breathing. This has indicated the promise of in-ear PPG as a means for both screening and ambulatory monitoring of patients with respiratory disorders, and as a tool for detailed breathing analysis in consumer wearables which goes beyond just respiration frequency.

Acknowledgment

This work was supported by the Racing Foundation grant 285/2018, MURI/EPSRC grant EP/P008461, MARVELS DoD grant, the Dementia Research Institute at Imperial College London, the Imperial Health Charity, the Imperial Biomedical Research Centre of the National Institute of Health Research, the British Heart Foundation, Pfizer Independent Grants, NHSX and the Rosetrees Foundation.

References

[1] D. Looney, A. Hemakom, and D. P. Mandic, "Intrinsic multi-scale analysis: A multi-variate empirical mode decomposition framework," *Proceedings of the Royal Society A: Mathematical, Physical and Engineering Sciences*, vol. 471, no. 2173, Jan 2015.

[2] L. Nilsson, A. Johansson, and S. Kalman, "Respiratory variations in the reflection mode photoplethysmographic signal. Relationships to peripheral venous pressure," *Medical and Biological Engineering and Computing*, vol. 41, no. 3, pp. 249–254, May 2003.

[3] L. M. Nilsson, "Respiration Signals from Photoplethysmography," *Anesthesia & Analgesia*, vol. 117, no. 4, pp. 859–865, Oct 2013.

[4] D. J. Meredith, D. Clifton, P. Charlton, J. Brooks, C. W. Pugh, and L. Tarassenko, "Photoplethysmographic derivation of respiratory rate: A review of relevant physiology," *Journal of Medical Engineering & Technology*, vol. 36, no. 1, pp. 1–7, Mar 2012.

[5] F. Yasuma and J. I. Hayano, "Respiratory Sinus Arrhythmia: Why Does the Heartbeat Synchronize with Respiratory Rhythm?" *Chest*, vol. 125, no. 2, pp. 683–690, Feb 2004.

[6] P. Dehkordi, A. Garde, B. Molavi, J. M. Ansermino, and G. A. Dumont, "Extracting Instantaneous Respiratory Rate From Multiple Photoplethysmogram Respiratory-Induced Variations," *Frontiers in Physiology*, vol. 9, no. JUL, p. 948, Jul 2018.

[7] L. Bernardi, A. Radaelli, P. L. Solda', A. J. Coats, M. Reeder, A. Calciati, C. S. Garrard, and P. Sleight, "Autonomic control of skin microvessels: Assessment by power spectrum of photoplethysmographic waves," *Clinical Science*, vol. 90, no. 5, pp. 345–355, 1996.

[8] O. S. Hoilett, A. M. Twibell, R. Srivastava, and J. C. Linnes, "Kick LL: A Smartwatch for Monitoring Respiration and Heart Rate using Photoplethysmography," in *Proceedings of the Annual International Conference of the IEEE Engineering in Medicine and Biology Society, EMBS*. IEEE, Jul 2018, pp. 3821–3824.

[9] S. Singh, M. Kozłowski, I. García-López, Z. Jiang, and E. Rodriguez-Villegas, "Proof of concept of a novel neck-situated wearable ppg system for continuous physiological monitoring," *IEEE Transactions on Instrumentation and Measurement*, vol. 70, pp. 1–9, 2021.

[10] D. Jarchi, D. Salvi, L. Tarassenko, and D. A. Clifton, "Validation of instantaneous respiratory rate using reflectance ppg from different body positions," *Sensors*, vol. 18, no. 11, 2018.

[11] E. L'Her, Q. T. N'Guyen, V. Pateau, L. Bodenes, and F. Lellouche, "Photoplethysmographic determination of the respiratory rate in acutely ill patients: Validation of a new algorithm and implementation into a biomedical device," *Annals of Intensive Care*, vol. 9, no. 1, p. 11, Dec 2019.

[12] D. Clifton, G. J. Douglas, P. S. Addison, and J. N. Watson, "Measurement of respiratory rate from the photoplethysmogram in chest clinic patients," *Journal of Clinical Monitoring and Computing*, vol. 21, no. 1, pp. 55–61, Feb 2007.

[13] K. H. Chon, S. Dash, and K. Ju, "Estimation of Respiratory Rate From Photoplethysmogram Data Using Time-Frequency Spectral Estimation," *IEEE Transactions on Biomedical Engineering*, vol. 56, no. 8, pp. 2054–2063, 2009.

[14] A. Johansson and P. Å. Öberg, "Estimation of respiratory volumes from the photoplethysmographic signal. Part 2: A model study," *Medical and Biological Engineering and Computing*, vol. 37, no. 1, pp. 48–53, 1999.

[15] S. Khreis, D. Ge, H. A. Rahman, and G. Carrault, "Breathing Rate Estimation Using Kalman Smoother with Electrocardiogram and Photoplethysmogram," *IEEE Transactions on Biomedical Engineering*, vol. 67, no. 3, pp. 893–904, Mar 2020.

[16] J. Li, J. Jin, X. Chen, W. Sun, and P. Guo, "Comparison of respiratory-induced variations in photoplethysmographic signals," *Physiological Measurement*, vol. 31, no. 3, pp. 415–425, Feb 2010.

[17] K. H. Shelley, D. H. Jablonka, A. A. Awad, R. G. Stout, H. Rezkanna, and D. G. Silverman, "What Is the Best Site for Measuring the Effect of Ventilation on the Pulse Oximeter Waveform?" *Anesthesia & Analgesia*, vol. 103, no. 2, pp. 372–377, Aug 2006.

[18] K. Budidha and P. A. Kyriacou, "In vivo investigation of ear canal pulse oximetry during hypothermia," *Journal of Clinical Monitoring and Computing*, vol. 32, no. 1, pp. 97–107, Feb 2018.

[19] L. Nilsson, T. Goscinski, S. Kalman, L.-G. Lindberg, and A. Johansson, "Combined photoplethysmographic monitoring of respiration rate and pulse: a comparison between different measurement sites in spontaneously breathing subjects," *Acta Anaesthesiologica Scandinavica*, vol. 51, no. 9, pp. 1250–1257, Aug 2007.

[20] W. P. Santamore and J. N. Amoore, "Buffering of respiratory variations in venous return by right ventricle: A theoretical analysis," *American Journal of Physiology - Heart and Circulatory Physiology*, vol. 267, Dec 1994.

[21] P. H. Charlton, T. Bonnici, L. Tarassenko, J. Alastruey, D. A. Clifton, R. Beale, and P. J. Watkinson, "Extraction of respiratory signals from the electrocardiogram and photoplethysmogram: Technical and physiological determinants," *Physiological Measurement*, vol. 38, no. 5, pp. 669–690, Mar 2017.

[22] L. Nilsson, T. Goscinski, A. Johansson, L. G. Lindberg, and S. Kalman, "Age and gender do not influence the ability to detect respiration by photoplethysmography," *Journal of Clinical Monitoring and Computing*, vol. 20, no. 6, pp. 431–436, Oct 2006.

[23] V. Goverdovsky, W. Von Rosenberg, T. Nakamura, D. Looney, D. J. Sharp, C. Papavassiliou, M. J. Morrell, and D. P. Mandic, "Hearables: Multimodal physiological in-ear sensing," *Scientific Reports*, vol. 7, no. 1, pp. 1–10, Dec 2017.

[24] D. Looney, P. Kidmose, C. Park, M. Ungstrup, M. Rank, K. Rosenkranz, and D. Mandic, "The in-the-ear recording concept: User-centered and wearable brain monitoring," *IEEE Pulse*, vol. 3, no. 6, pp. 32–42, 2012.

[25] T. Nakamura, Y. D. Alqurashi, M. J. Morrell, and D. P. Mandic, "Hearables: Automatic Overnight Sleep Monitoring with Standardized In-Ear EEG Sensor," *IEEE Transactions on Biomedical Engineering*, vol. 67, no. 1, pp. 203–212, Jan 2020.

[26] G. Hammour, M. Yarici, W. V. Rosenberg, and D. P. Mandic, "Hearables: Feasibility and Validation of In-Ear Electrocardiogram," in *Proceedings of the Annual International Conference of the IEEE Engineering in Medicine and Biology Society, EMBS*. IEEE, Jul 2019, pp. 5777–5780.

[27] B. Venema, N. Blanik, V. Blazek, H. Gehring, A. Opp, and S. Leonhardt, "Advances in reflective oxygen saturation monitoring with a novel in-ear sensor system: Results of a human hypoxia study," *IEEE Transactions on Biomedical Engineering*, vol. 59, no. 7, pp. 2003–2010, 2012.

[28] B. Venema, J. Schiefer, V. Blazek, N. Blanik, and S. Leonhardt, "Evaluating Innovative In-Ear Pulse Oximetry for Unobtrusive Cardiovascular and Pulmonary Monitoring During Sleep," *IEEE Journal of Translational Engineering in Health and Medicine*, vol. 1, pp. 2 700 208–2 700 208, Aug 2013.

[29] H. J. Davies, I. Williams, N. S. Peters, and D. P. Mandic, "In-Ear SpO2: A Tool for Wearable, Unobtrusive Monitoring of Core Blood Oxygen Saturation," *Sensors*, vol. 20, no. 17, p. 4879, Aug 2020.

[30] M. Xie, X. Liu, X. Cao, M. Guo, and X. Li, "Trends in prevalence and incidence of chronic respiratory diseases from 1990 to 2017," *Respiratory Research*, vol. 21, no. 1, p. 49, Feb 2020.

[31] N. Snell, D. Strachan, R. Hubbard, J. Gibson, E. Limb, R. Gupta, A. Martin, M. Laffan, and I. Jarrold, "Burden of lung disease in the UK; findings from the British Lung Foundation's "respiratory health of the nation" project," in *European Respiratory Journal*, vol. 48, no. suppl 60. European Respiratory Society (ERS), Sep 2016, p. PA4913.

[32] G. Viegi, F. Pistelli, D. L. Sherrill, S. Maio, S. Baldacci, and L. Carrozzi, "Definition, epidemiology and natural history of COPD," *European Respiratory Journal*, vol. 30, no. 5, pp. 993–1013, Nov 2007.

[33] M. J. Tobin, T. S. Chadha, G. Jenouri, S. J. Birch, H. B. Gazeroglu, and M. A. Sackner, "Breathing Patterns: 2. Diseased Subjects," *Chest*, vol. 84, no. 3, pp. 286–294, 1983.

[34] H. Wilkens, B. Weingard, A. Lo Mauro, E. Schena, A. Pedotti, G. W. Sybrecht, and A. Aliverti, "Breathing pattern and chest wall volumes during exercise in patients with cystic fibrosis, pulmonary fibrosis and COPD before and after lung transplantation," *Thorax*, vol. 65, no. 9, pp. 808–814, 2010.

[35] A. M. Russell, H. Adamali, P. L. Molyneaux, P. T. Lukey, R. P. Marshall, E. A. Renzoni, A. U. Wells, and T. M. Maher, "Daily home spirometry: An effective tool for detecting progression in idiopathic pulmonary fibrosis," *American Journal of Respiratory and Critical Care Medicine*, vol. 194, no. 8, pp. 989–997, Oct 2016.

[36] K. K. Dames, A. J. Lopes, and P. L. De Melo, "Airflow pattern complexity during resting breathing in patients with COPD: Effect of airway obstruction," *Respiratory Physiology and Neurobiology*, vol. 192, no. 1, pp. 39–47, Feb 2014.

[37] S. A. Shah, C. Velardo, A. Farmer, and L. Tarassenko, "Exacerbations in chronic obstructive pulmonary disease: Identification and prediction using a digital health system," *Journal of Medical Internet Research*, vol. 19, no. 3, p. e69, Mar 2017.

[38] H. Yamazaki and K. Fujimoto, "A new noninvasive method for measurement of dynamic lung compliance from fluctuations on photoplethysmography in respiration," *Journal of Applied Physiology*, vol. 130, no. 1, pp. 215–225, Jan 2021.

[39] V. Goverdovsky, D. Looney, P. Kidmose, and D. P. Mandic, "In-Ear EEG From Viscoelastic Generic Earpieces: Robust and Unobtrusive 24/7 Monitoring," *IEEE Sensors Journal*, vol. 16, no. 1, pp. 271–277, Jan 2016.

[40] H. J. Davies, G. Hammour, and D. P. Mandic, "An apparatus for the simulation of breathing disorders: Physically meaningful generation of surrogate data," *arXiv preprint arXiv:2109.06699*, Sep 2021.

[41] T. M. Rutkowski, J. Dauwels, F. Vialatte, A. Cichocki, and D. P. Mandic, "Time-frequency and synchrony analysis of responses to steady-state auditory and musical stimuli from multichannel EEG."

[42] D. Looney, C. Park, Y. Xia, P. Kidmose, M. Ungstrup, and D. P. Mandic, "Towards estimating selective auditory attention from EEG using a novel time-frequency-synchronisation framework," in *Proceedings of the International Joint Conference on Neural Networks*, 2010, pp. 1–5.

[43] K. V. Madhav, M. R. Ram, E. H. Krishna, N. R. Komalla, and K. A. Reddy, "Estimation of respiration rate from ECG, BP and PPG signals using empirical mode decomposition," in *Conference Record - IEEE Instrumentation and Measurement Technology Conference*, 2011, pp. 1661–1664.

[44] N. Ur Rehman, C. Park, N. E. Huang, and D. P. Mandic, "EMD via MEMD: Multivariate noise-aided computation of standard EMD," *Advances in Adaptive Data Analysis*, vol. 05, no. 02, p. 1350007, Apr 2013.

[45] N. Rehman and D. P. Mandic, "Multivariate empirical mode decomposition," *Proceedings of the Royal Society A: Mathematical, Physical and Engineering Sciences*, vol. 466, no. 2117, pp. 1291–1302, May 2010.

[46] F. Pedregosa, G. Varoquaux, A. Gramfort, V. Michel, B. Thirion, O. Grisel, M. Blondel, P. Prettenhofer, R. Weiss, V. Dubourg, J. Vanderplas, A. Passos, D. Cournapeau, M. Brucher, M. Perrot, and É. Duchesnay, "Scikit-learn: Machine Learning in Python," *Journal of Machine Learning Research*, vol. 12, no. Oct, pp. 2825–2830, 2011.